Results in Surfaces and Interfaces 21 (2025) 100645

Contents lists available at ScienceDirect

Results in Surfaces and Interfaces

journal homepage: www.elsevier.com/locate/rsurfi

Hydrolysate from leather tanning waste as clay modifier for pig manure treatment

Marianna Guagliano [a,*], Andrea Tong Hua Borgonovo [a,b], Silvia Mostoni [c], Maria Lacalamita [d], Ernesto Mesto [d], Elisabetta Finocchio [e], Giovanni Dotelli [a], Emanuela Schingaro [d], Stefania Lupinelli [f], Serena Reggi [g], Matteo Dell'Anno [g,h], Luciana Rossi [g], Roberto Scotti [c,i], Maurizio Bellotto [j], Cinzia Cristiani [a]

[a] Department of Chemistry, Materials and Chemical Engineering "Giulio Natta", Politecnico di Milano, Piazza Leonardo Da Vinci 32, 20133 Milano, Italy
[b] Perfetti Van Melle Italia, Via A. Clerici, 30, 20045 Lainate, MI, Italy
[c] Department of Materials Science, INSTM, Università degli Studi di Milano-Bicocca, Via R. Cozzi 55, 20125, Milano, Italy
[d] Department of Earth Science and Geoenvironmental, Università degli Studi di Bari Aldo Moro, Bari 70125, Italy
[e] Department of Civil, Chemical and Environmental Engineering—DICCA, Università di Genova (UniGe), Via All'Opera Pia 15, 16145 Genova, Italy
[f] ILSA S.p.A, Via Quinta Strada 28, 36071, Arzignano, Italy
[g] Department of Veterinary Medicine and Animal Sciences—DIVAS, Università degli Studi di Milano, via dell'Università 6, 26900 Lodi, Italy
[h] Department of Veterinary Sciences, Università degli Studi di Messina, Viale Giovanni Palatucci 13, 98168, Messina, Italy
[i] Institute for Photonics and Nanotechnologies-CNR, Via Alla Cascata 56/C, Povo, 38123, Trento, TN, Italy
[j] Opigeo S.r.l, Via dell'Industria, 13, 36040, Grisignano di Zocco, VI, Italy

ARTICLE INFO

Keywords:
Waste valorisation
Leather industry waste
Adsorption
Cu(II)
Zn(II)
Swine manure
Water polluted streams remediation

ABSTRACT

The heavy metals pollution from agricultural waste is a significant concern. Among these, zinc and copper are prevalent pollutants that can be found in pig manure.

The application of sorbents has emerged as a pivotal strategy for the effective removal of these pollutants from manure. One of the most well-known and widely used sorbents are clays and organoclays. In this work, both pristine Ca-montmorillonite (STx) and protein-functionalized Ca-montmorillonite (STx-HY) are tested as sorbents for Zn and Cu capture. Protein-functionalized organoclay was obtained by treating Ca-montmorillonite with two types of collagen hydrolysate (HY), the by-product of the leather tanning process (supplied by Ilsa Group). The synthesis of STx-HY was accomplished via a solid/liquid adsorption process in mild conditions. An uptake plateau was found corresponding to a loading of 0.42–0.44 $mmol_{HY}/g_{STx}$. The metal uptake efficiencies of clay and organoclays were tested in solutions simulating the concentration of Cu and Zn in weaning pig's manure. The results obtained demonstrated near-total capture at 0.06 $mmol_{Cu}/g_{STx}$, irrespective of the sorbent used. Furthermore, an increase in HY loadings resulted in enhanced Cu capture at 0.38 $mmol_{Cu}/g_{STx}$, suggesting a saturation point of 2.00 $mmol_{Cu}/g_{STx}$ for both hydrolysates, corresponding to a maximum Cu capture of 0.45 $mmol_{Cu}/g_{STx}$ and 0.6 $mmol_{Cu}/g_{STx}$. In case of zinc, a maximum metal capture of 0.4–0.5 $mmol_{Zn}/g_{STx}$ was obtained by both pristine and modified STx.

1. Introduction

Despite the considerable progress made in recent years by modern pig farming systems to comply with European regulations on animal welfare and reduction of antibiotics use, the presence of heavy metals in manure remains a significant issue [1–4], contributing to environmental problems [1,5,6]. Although, zinc and copper are essential nutrients required for the formulation of animal diets [7], their inorganic salts have relatively limited bioavailability, and as a result, they are excreted in considerable amounts in manure [8,9]. A study on the animal rearing system in northern Italy indicated an average concentration in pig faeces during weaning of 3385 mg/kg of zinc and 205.72 mg/kg of copper [10].

Their accumulation in agricultural soils can compromise land

* Corresponding author.
E-mail address: marianna.guagliano@polimi.it (M. Guagliano).

https://doi.org/10.1016/j.rsurfi.2025.100645
Received 13 May 2025; Received in revised form 24 September 2025; Accepted 24 September 2025
Available online 6 October 2025

suitability for crops due to their potential hazardous effects on human consumers because of excessive accumulation of heavy metals [11–14].

Pig slurry, composed of manure particles suspended in water, can be purified using various wastewater treatment methods, including metal ion capture via filtration through a material such as charcoal, zeolites [15], or clays such as montmorillonite. However, sorbents are prone to some limitations, such as low binding capacity and low selectivity towards metals [16], and these properties can be improved via solids modification [17]. Among others, organoclays have successfully been applied for removing organic compounds, metallic cations and anions, inorganic anions and pharmaceutical compounds from water solution [18,19]. Different natural and synthetic organo-modifiers have been proposed in the literature [20]. In the context of a more responsible consumption of natural resources, a greener and environmentally friendly chemistry, studies have identified the potential of modified natural and eco-friendly materials to remediate wastewater from pollutants. For instance, clays such as natural calcium montmorillonite and Layered Double Hydroxides (LDH) modified with amino acids have been recently proposed for remediation of mining wastewaters [21]. Extensive research has been performed on the adsorption of specific types of amino acids such as pure arginine and glycine into Montmorillonite [22–24]. It is reported that smectites can interact with either the amide or carboxyl groups of non-charged amino acids, leading to the expansion of interlayer space to accommodate them [25,26]. In this respect, a waste-aminoacidic resource, such as flesh residue from leather tanning, could be of high interest. This residue is the conversion of animal hides into leather via a complex sequence of chemical reactions and processes including trimming, fleshing, splitting, and shaving [27]. As a matter of fact, the leather industry incurs a significant amount of animal waste by-product. While steps have been taken to reduce waste generation, according to one metric, for each ton of wet salted hide only 200 Kg of leather is obtained, with over 600 Kg of solid waste, constituted mostly of animal flesh and chromium-containing tannery wastes [28]. The flesh waste is mostly present in the form of collagen, free fatty acids and fleshing, which are undesired meat trimmings from the skins [29], and constitutes around 50–60 % of tannery solid waste [7]. The solid waste generated in this industry can pose a major problem to the environment without proper treatment [30] and an estimated 979,800 tons of fleshing waste is generated worldwide each year [31]. Despite being considered waste, these fleshing contain large amounts of valuable biomolecules such as lipids (7–15 %) and proteins (50–60 %) [31].

In this scenario, within the optic of a circular economy and the growing global consciousness regarding sustainable practices, an ideal organoclay would utilize waste biomaterial as its protein resource. The use of waste material in production processes can lead to a lengthening of the availability of remaining resources, and it is necessary considering the notable global decrease in abundance of materials [32].

This study proposes the preparation, characterization and testing towards Cu and Zn capture of an innovative organoclays, functionalized via the use of two hydrolysed amino acid solutions, obtained from waste in the leather industry (provided by ILSA S.p.A) with the aim to improve the clay's ability to capture copper and zinc ions in aqueous streams with concentrations similar to those of pig farming wastewater, promoting their circular reuse within the agricultural industry.

The functionalization was performed according to a previously developed [33] simple and environmentally friendly solid/liquid adsorption procedure, which is performed without any modification of the waste-derived hydrolysates, in aqueous solution and room temperature.

The solids were fully characterized with the attempt to find a correlation between the preparation process and the heavy metals removal capability.

The final goal of this paper is to demonstrate the potential use of waste-derived materials for environmental preservation. Indeed, it proposes an approach that involves the use of one type of waste (the hydrolysates, in this case) to treat another waste (water polluted by heavy metals), thereby achieving a double valorisation of waste materials and promoting the responsible use of natural resources, including water.

2. Experimental

2.1. Materials

As support, the Ca-montmorillonite (STx-1b which stands for "State of Texas", STx), supplied by the US Clay Minerals Society Source Clay Repository, was used. The clay has a white colour, and a crystal formula $^{XII}(Ca_{0.14}Na_{0.02}K_{0.01})^{VI}(Al_{1.21}Fe^{3+}_{0.05}Mg^{2+}_{0.36}Ti_{0.02})^{IV}Si_{4.0}O_{10}(OH)_2$. It is supplied as dry powder, pre-processed by sieving to select the ≤44 μm fraction. It is characterized by a surface area of 83.79 ± 0.22 m^2/g [34].

For all the experiments, the pristine powder, without any treatment, was used; however, in-depth investigations were carried out on the ≤2 μm fraction, separated by gravity setting, according to the procedure described in [35].

As clay modifiers two hydrolysed amino acid mixtures (HY, hereafter) obtained from waste of leather tanning process [28], (supplied by ILSA S.p.A (Arzignano (VI), Italy) were applied, namely.

- *A3001* (***A***, hereafter) is a brown-coloured liquid, characterized by a molecular weight of 1327 g/mol, a degree of hydrolysis of 11 %, a free amino acids content of 0.9 %, and a Ca content of 0.695 mg/g (0.017 mmol/g)
- *DE5032 (***DE**, hereafter) is a dark brown-coloured liquid, characterized by a molecular weight of 1937 g/mmol, a degree of hydrolysis of 23.7 %, a free amino acids content of 10.3 %, and a Ca content of 0.5126 mg/g (0.013 mmol/g).

The total amount of amino acids in the two collagen hydrolysate of high molecular weight is provided in Table S1. Glycine, proline, hydroxyproline, glutamic acid, arginine, and alanine are the main component.

2.2. Methods

2.2.1. Organoclay preparation

Organoclays (STx-HY, in the following) were prepared via solid/liquid adsorption (Fig. 1), according to a procedure developed elsewhere [33,36]. Typically, a fixed amount of STx (2.5 g) was contacted with 50 mL of the HY solution (0.3–7.2 $mmol_{HY}/g_{STx,}$ corresponding to a molar concentration of 15–360 mM), at room temperature, stirring for 90 min at 500 rpm. pH was monitored during the experiment (glass electrode, pH-meter Fiveeasy F20-std-kit Mettler Toledo), but no pH correction was done. The measured pH during the organoclay preparation was 5.2–6.6 for *A* hydrolysate and 5.6–6.2 for *DE*.

Finally, the solids and the liquids were separated by centrifugation (12 min at 1008 RFC) and fully characterized.

Adsorbed HY was determined before and after the contacting experiments by Chemical Oxygen Demand (COD, hereafter). Analyses were performed by HI80 Spectrophotometer (Hanna Instrument), according to O'Dell [37]). The adsorbed HY was calculated according to Eq. (1):

$$HY_{ads}\left(mmol_{HY}/g_{STx}\right) = \left[HY_{ini}\left(mmol_{HY}/g_{STx}\right) - HY_{res}\left(mmol_{HY}/g_{STx}\right)\right] \quad (1)$$

where: "HY_{ads}" is the amount of adsorbed hydrolysate, "HY_{ini}" and "HY_{res}" are the amount of hydrolysate in solution before and after the uptake reaction, respectively. Analyses were performed in duplicate on selected samples with an error between ±0.007 and ± 0.16 mmol/g, depending on the initial HY amount.

The solids were dried at room temperature overnight, ground up, and characterized by physio-chemical analysis.

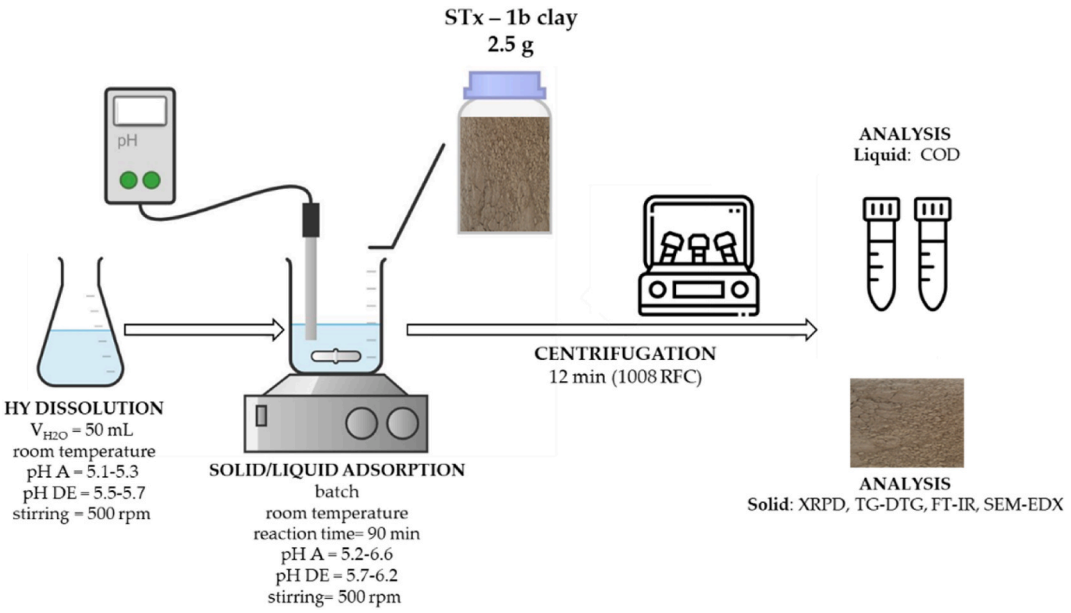

Fig. 1. Scheme of the organoclays preparation procedure.

In the following, the synthetized organoclays are identified with a label indicating the type and the amount of HY loaded on STx. For example, STx-A 0.3 represents the organoclay prepared with ***A*** hydrolysate (25 mM) which loaded 0.3 mmol of HY per gram of clay.

2.2.2. Metal ions uptake experiments

The obtained organoclays were then tested for metal capture in simulated solutions containing Cu(II) and Zn(II) ions.

For this purpose, simulated solutions were prepared by dissolving $Cu(NO_3)_2{*}3H_2O$ and $Zn(NO_3)_2{*}\ 6H_2O$ (both supplied by Sigma Aldrich) in distilled water. Three copper solutions 3.3, 19 and 100 mM, (corresponding to 0.06, 0.38 and 2 $mmol_{Cu}/g_{STx}$, respectively), and one zinc solution 52 mM (corresponding to 1.03 mmol $_{zn}/g_{STx}$) have been tested. The concentrations of Cu (3.3 mM) and Zn (52 mM) correspond to Cu and Zn in weaning pig manure, respectively [10,38].

The contacting reaction was performed by following the same procedure shown of Fig. 1. In a typical experiment (Fig. S1), 1g of organoclay was contacted with 50 mL of the metal ions solution. All adsorption reactions were performed at room temperature, stirring time of 90 min at 500 rpm, monitoring the pH during the experiment, but without correction. The pH of the copper suspensions varied between 4.7 and 3.3, while that of the Zn suspensions between 4.9 and 5.5.

Finally, the solids and the liquids were separated by centrifugation (12 min, 1008 RFC).

Copper solutions were analysed spectrophotometrically (H1801 Spectrophotometer, Hanna Instruments), while zinc solutions were analysed by Inductively Coupled Plasma Optical Emission Spectroscopy (ICP, PerkinElmer OPTIMA 7000 DV spectrometer PerkinElmer, Waltham, MA, United States). Analyses were performed in duplicate on selected samples, and the analytical error was ±0.002–0.16 mmol/g $_{STx}$).

The adsorbed ions were calculated according to Eq. (2):

$$M(II)_{ads}\left(mmol_{cu}/g_{Carrier}\right) = \left[M(II)_{ini}\left(mmol_{Cu}/g_{Carrier}\right) - M(II)_{res}\left(mmol_{Cu}/g_{Carrier}\right)\right] \quad (2)$$

where: "M(II)" is Cu(II) or Zn(II), "M(II)ads" the amount of captured metal ion, "$M(II)_{ini}$", and "$M(II)_{res}$" are the amount of metal ion in solution before and after the uptake reaction, respectively. An analytical error of ±3 % was found.

The solids, after metal adsorption, were dried at room temperature overnight, ground up into a fine powder, and fully characterized by physical-chemical analyses.

Hereafter, the organoclays are identified with a label indicating the organoclay composition and the amount of heavy metal captured per gram of carrier. For example, the label STx-A0.4-Cu0.45 identifies the organoclay loaded with 0.4 mmol per gram of HY which captured 0.45 mmol of Cu per gram of sorbent.

2.2.3. Solids characterization

The pristine clay and the organoclays were fully characterized before and after metal uptake.

X-ray powder diffraction analysis (XRPD) was performed by means of a PANalytical Empyrean diffractometer equipped with a 1.8 kW CuKα ceramic X-ray tube and a Real Time Multiple Strip (RTMS) PIXcel3D detector. Operating conditions were: 40 mA and 40 kV; step size 0.0263°; counting time 297 s per step. The incident beam pathway included a 0.063° divergence slit, a 0.125° antiscatter slit and 0.02 rad Soller slits, whereas a Ni filter, 0.02 rad Soller slits and an antiscatter slit (7.5 mm) were mounted in the diffracted pathway. Patterns were collected on side-loaded mounts in the 2θ range 4–80°. *Small-angle X-ray scattering (SAXS)* was also employed for measurements at small angle (0.5–7° 2θ range) of the ≤2 μm fraction. In this case, the sample was loaded in a 0.5 mm capillary and the instrument operated in transmission geometry to measure the intensity of X-rays scattered from the sample in the immediate vicinity of the direct beam. A focusing X-ray mirror with 0.031° divergence slit and a 0.125° antiscatter slit was mounted on the incident beam pathway, whereas an antiscatter slit (0.1 mm) was used in the diffracted pathway. The data were collected with a step size of 0.02° and a counting time of 35 s per step.

Fourier Transform-InfraRed (FT-IR) in Attenuated Total Reflectance

mode (FTIR-ATR). Spectra of pristine and synthesized organoclay have been collected in the MID-IR region using a Thermonicolet Nexus FT IR instrument equipped with ATR accessory (diamond window). Applied analysis parameters: 100 scans, 4 cm^{-1} resolution, DTGS detector, background air.

Scanning electron microscopy and energy dispersive X-ray spectroscopy (SEM-EDX) analysis were performed by a Zeiss EVO 50 EP (Zeiss, Jena, Germany) combined with a spectrometer Oxford INCA energy 2000 (Oxford Instruments, Abingdon, UK). The SEM-EDX equipment was operated at an electron high tension (EHT) voltage of 15 and 20 kV, a current probe of 120 and 300 pA, and at high vacuum (about 10^{-4} Pa) to acquire images from both secondary and electrons chemical mapping.

Thermogravimetric analysis (TG-DTG). Thermal decomposition was analysed by thermogravimetric and differential thermogravimetric Analysis (TG-DTG) with a DTA-TG SEIKO 6300 instrument (Seiko Instruments Inc., Chiba, Japan), from room temperature up to 800 °C in air, heating rate of 10 °C/min.

Electron Paramagnetic Resonance (EPR) analyses were conducted to evaluate the Cu^{2+} adsorption in the organoclay contacted with Cu (initial amount corresponding to 2 $mmol_{cu}/g_{clay}$). EPR measurements were performed at 123 K by using a Bruker EMX spectrometer operating at the X-band frequency and equipped with an Oxford cryostat. Spectra were recorded at a power of 2 mW, modulation amplitude 2 or 10 G, and at 130 K.

3. Results and discussion

3.1. Carrier characterization

STx clay has been widely characterized in literature [38,39]; however, for sake of completeness, the analysis of the pristine carrier was also performed, by means of XRPD, TG, FTIR and SEM-EDX.

In the XRPD pattern (Fig. S2), the characteristic, well-defined basal reflection at 5.79 2θ° was observed. The sharpness and intensity of the basal reflection confirmed the degree of the stacking order. A calculated *d001* spacing of 15.25 Å was found, in line with literature [38].

The two intense phenomena in TG-DTG analysis (Fig. S3a and b), in the range 100–110 °C, are related to water release, physisorbed and coordinated, respectively, whereas the broad phenomenon between 550 and 750 °C is consistent with de-hydroxylation and clay collapse [40].

FT-IR spectra recorded in ATR mode are reported in Fig. S4. The main features of the spectra correspond to stretching modes of structural hydroxyl groups (3620 cm^{-1}), stretching modes of Si-O (989-800 cm^{-1}), deformation bands of Al-Al-OH groups (917 cm^{-1}) and of Al-Mg-OH groups (842 cm^{-1}). Moreover, coupled out-of-plane vibration bands of Al-O and Si-O (625 cm^{-1}), and Al-O-Si deformation bands (525 cm^{-1}) can be recognized, in accordance with literature [41].

STx was also investigated in terms of morphology and elemental composition by SEM-EDX analysis (Fig. S5 a,b). Morphologically, it presented agglomerates of different size in the range of 20–100 μm (Fig. S5a), with some irregularities on their surface. From EDX analysis (Fig. S4b), STx components were Silicon (Si), Aluminium (Al), Oxygen (O), Magnesium (Mg) and Calcium (Ca), as evidenced by the EDX spectra (Fig. S5b).

3.2. Organoclay synthesis

The uptake, (analysis error in the range ± 0.007 and ± 0.16 mmol/g), of *A* and *DE* hydrolysates by STx as function of the initial HY concentration is plotted in Fig. 2a and b.

Considering the adsorption curve of ***A*** hydrolysate, an increasing linear trend was observed with the initial concentration range of 0.3–0.8 $mmol/g_{STx}$. A further increase in ***A*** initial content (1.4–1.8 $mmol/g_{STx}$) did not result in a higher ***A*** loading, but in reaching an adsorption plateau of 0.42–0.44 ± 0.06 $mmol_{HY}/g_{STx}$. Moreover, when ***A*** initial content is further increased up to 8 $mmol_{HY}/g_{STx}$, an almost linear behaviour occurred. On the contrary, ***DE*** adsorption trend was always linear for all the investigated initial concentration range (0.5–3.6 $mmol_{DE}/g_{STx}$, Fig. 2a).

The presence of a threshold value in ***A*** hydrolysate adsorption can be better evidenced when the adsorption efficiency is considered (Fig. 2b). It is evident that a progressive decrease in ***A*** loading efficiency from 80 to 20 % (w/w) occurred on increasing ***A*** content in the contacting solution, while for DE constant loading efficiency at about 30–40 % (w/w) was calculated. Accordingly, a sites saturation mechanism can be hypothesized for the adsorption of both the hydrolysates, where the saturation of the adsorption sites is immediately reached for ***DE***, but not for ***A***.

The amount of amino acids and peptides loaded by the clay can vary considerably depending on the peptide nature. For example, Sippy Kalra et al. [42] observed that an increasing in the chain length of glycine polymers resulted in an increased adsorption when Ca/Mg and neutral montmorillonite were used. Moreover, the adsorption showed a typical Langmuir-type asymptotic trend, explained by considering the peptide/polypeptide equilibrium concentration in solution. Therefore, the amount of the adsorbed molecule increases up to a certain limit, which corresponds to the saturation point; once exceeded this threshold value, the adsorption process becomes independent on the molecule's initial concentration. This behaviour was demonstrated both for small peptides, such as di-amino acids and for larger molecules, as

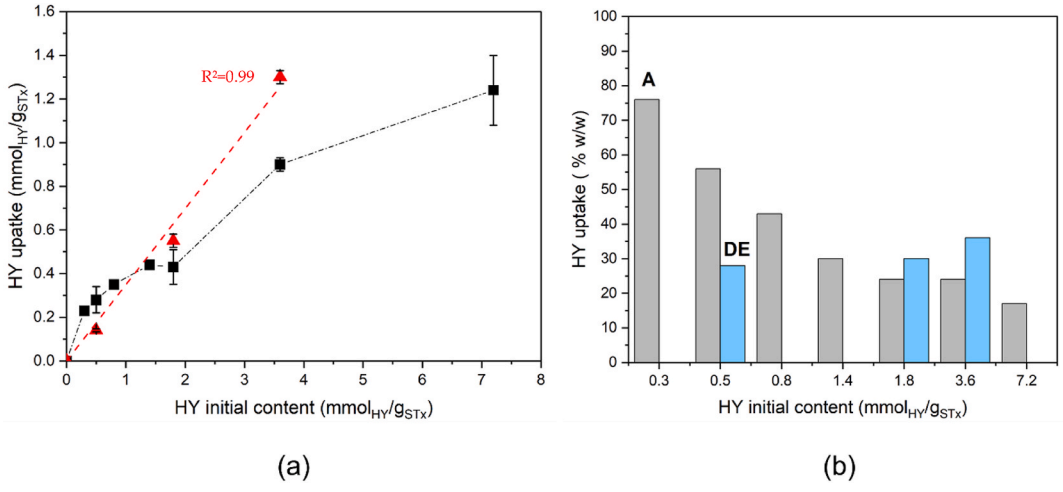

Fig. 2. HY uptake as function of HY initial content: a) absolute values and b) capture efficiency (black square ***A***, red triangle ***DE***).

betalactoglobuline [43]. Furthermore, regarding ***A*** adsorption behaviour, the presence of a two steps process consisting of a plateau followed by an almost linear trend was also observed by Anita Parbhakar et al. [44] in the adsorption of L-lysine on Na-montmorillonite. In this case the adsorbate binds to the substrate, whereby a concentration is reached that allows for an attractive interaction between the adsorbing molecules, thus promoting an enhanced adsorption process.

Additionally, in case of ***A***, the role of pH during adsorption cannot be discarded. Indeed, in the range 0.3–1.8 $mmol_A/g_{STx}$ the measured pH was about 6–6.6; in this pH range, the main constituent amino acids of the ***A*** hydrolysed, such as glycine, proline, hydroxyproline, are neutral or, at least, negatively charged, because, being their isoelectric points (IP) in the range 6–6.3, (Table S1), pH is higher than IP. When the ***A*** concentrations is increased, the pH value is 5.3, thus resulting in amino acids positively charged. Considering the negative charged STx surface [45,46], the further and large linear adsorption observed after the plateau can be explained with a Coulombic attraction interaction. Similar considerations can be applied to ***DE***, which constant adsorption efficiency could be related to a constancy in pH, stable at 5.7-6 throughout the experiment.

Accordingly, the different behaviour of ***A*** and ***DE*** can be explained considering a possible different polypeptide distribution in the hydrolysate, being them obtained by the hydrolysis of different wastes.

Regarding the adsorption mechanism, it is reported in the literature that the organic molecule can interact with montmorillonite in different ways, such as [47]: 1) intercalation with or without ion exchange; 2) surface adsorption. The knowledge of the adsorption mechanism is of paramount importance to understand the clay-molecule interaction strength, fundamental in the adsorption process.

To investigate the interaction mechanism, the synthesized organoclays were analysed by XRPD. The obtained patterns are plotted in Fig. 3, where pristine STx is reported for comparison.

By increasing the ***A*** initial content, a progressive shift and broadening of the (001) reflection towards lower angles ($2\theta = 4.97°$, $d = 17.85$ Å for the STx-A0.4 sample) occurred. A similar behaviour was observed for ***DE***-based organoclays ($2\theta = 4.83°$, $d = 18.28$ Å for the STx-DE0.55 sample). These results indicate an interlayer expansion up to maximum values of 2.60 and 3.03 Å for STx-A0.4 and STx-DE0.55, respectively. Moreover, by increasing the initial content of hydrolysates, a progressive increase of calcium release, up to 0.4 mmol/g was measured (Fig. S6). This value is in line with the cation exchange capacity (CEC) of 84.4 meq/100g, (corresponding to 0.422 mmol/g of Ca^{2+}) reported on the technical data sheet of the STx-1b [34]. The calcium release was calculated by the difference between the total Ca present in the solution after the contacting reaction and the Ca present in the pristine hydrolysed solution.

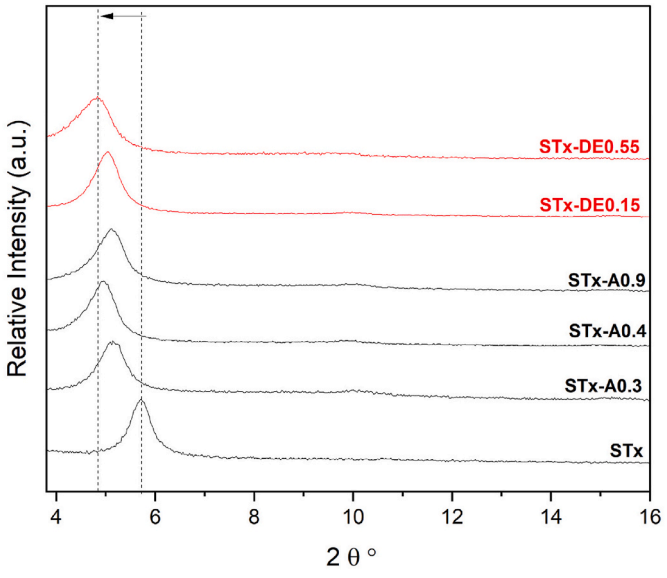

Fig. 3. XRPD patterns of the organoclays with different HY loadings, (pristine STx for sake of comparison).

The adsorption behaviour of the STx fraction ≤2 μm was also tested using the ***A*** hydrolysate. The HY loading of this clay fraction increases as a function of the HY initial content. In addition, a better HY loading capacity of the STx ≤2 μm with respect to the bulk STx was observed (Table S2). In this case, by increasing the HY content, a constant Ca ions release (0.16–0.17 $mmol_{Ca}/g_{STx}$) of the ≤2 μm clay fraction was found (Table S2). The small-angle X-ray diffraction pattern of the STx ≤2 μm evidences a broad (001) reflection at $2\theta \sim 4.8°$ and no additional peaks at lower Bragg's angles (Fig. S7). The interlayer expansion of the STx fraction ≤2 μm is similar to that of the bulk sample ($d \sim 18.6$ and 17.85 Å, respectively). Thus, it appears that the high reactivity and extent of uptake of the ≤2 μm fraction may be ascribed to its high specific surface area if compared with the bulk sample.

Therefore, all the studied organoclays, including the fraction ≤2 μm show a maximum interlayer expansion of about 3 Å. The same expansion was calculated for tyrosine [48]. A constant d-spacing was observed when Na-montmorillonite was contacted with arginine solutions of different concentrations [48], as well as in the cases of adsorption of glycine and cysteine, despite their different molecular structure [21] or of larger molecules such as beta-lactoglobulin (18.4 KDa) [43] and tryptone oligomers [25].

During our experiments, the concentration of ***A*** in solution was about 1–22 times the CEC of the used montmorillonite, while ***DE*** concentrations were about 1 and 6 times of CEC. Zhang et al. reported [49] that both intercalation and surface adsorption occur when the adsorption with molecular concentrations largely exceeds the CEC of the clay minerals.

In addition, given the dimensions and steric hindrance of the used HY, only free amino acids and/or parts of the polypeptides may be intercalated. On the other hand, the total HY loading higher than the CEC of the montmorillonite evidence the occurrence of surface adsorption. Both mechanisms suffer from site saturation, limited number of molecules allocable in the interlayer and limited number of surface sites.

The intercalation process can be also evaluated based on the water molecules release. Accordingly, the organoclays were characterized by TG-DTG measurements, and the obtained data were compared to those of the pristine clay (Fig. S8 and Fig. 4a and b). Thermal decomposition (TG, Fig. S3) of pristine STx is quite simple, the total weight loss occurs within 200 °C and it is associated with water release both physi- and chemi-sorbed water molecules; while the modulation of the curve at about 600 °C is associated with dehydroxylation of the layer [50,51].

When the clay is loaded with HY, a more complex situation appears, showing at least three decomposition phenomena, with associated weight losses (Fig. S8).

1) from room temperature up to 150 °C, with an associate weight loss of 15 %,
2) between 300 and 400 °C, with an associate weight loss in the range 10–16 %,
3) between 450 and 600 °C, with an associate weight loss in the range 14–22 %.

As in the samples the HY loading is very close, TG curves (Fig. S8) are almost overlapped, and for a better analysis of the phenomena, DTG curves were considered (Fig. 4)

All the samples of organoclay, regardless of the HY nature or concentration, showed a very similar DTG pattern. The two intense phenomena below 100 °C and around 110 °C in pristine STx, are related to water release, physisorbed and coordinated, respectively, as observed for the pristine sample [39]. The phenomena between 300 and 500 °C with a maximum at about 370 °C, the barely evident shoulders at about

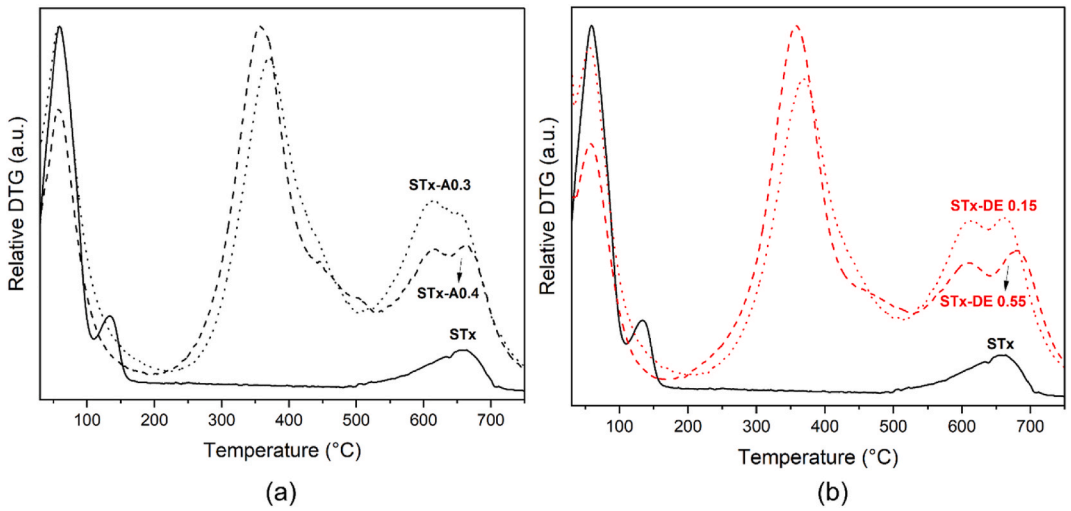

Fig. 4. DTG of the Organoclays: a) ***A***-based and b) ***DE***-based samples.

450 °C and 500 °C, as well as the shoulder at about 600 °C, not present in pristine STx, can be associated either with the decomposition of free amino acids [52,53] and/or collagen peptides when bonded to carbon-based materials, such as chitosan and functionalized multiwalled carbon nanotube [54]. All these molecules are HYs components, in particular collagen peptides, given the HYs animal origin. The presence of free amino acids and/or small peptides are also consistent with the decomposition temperature, as decomposition of free collagen is reported at about 300–350 °C, without any additional phenomena at higher temperature [55]. On the contrary, the high temperature shoulder (at about 600 °C) is an indication of collagen peptides interacting with C-based materials, for instance chitosan and functionalized multiwalled carbon nanotube [52,54,56].

Moreover, no coordinated water evolution (T = 110–120 °C) occurred in the organoclays (Fig. 4a and b), as expected in case of intercalation.

Once more, materials characterization points out the presence of small molecules (amino acids or peptides) interacting with the carrier, and partially intercalated.

Materials were also characterized by means of FTIR – ATR mode. In Fig. 5, the subtraction spectra of hybrid hydrolysate samples are reported. The spectrum of STx matrix has been subtracted to enhance the intensity of the hydrolysate IR bands. The reference spectra of both pure hydrolysate materials are also reported in Supporting Information (Fig. S9).

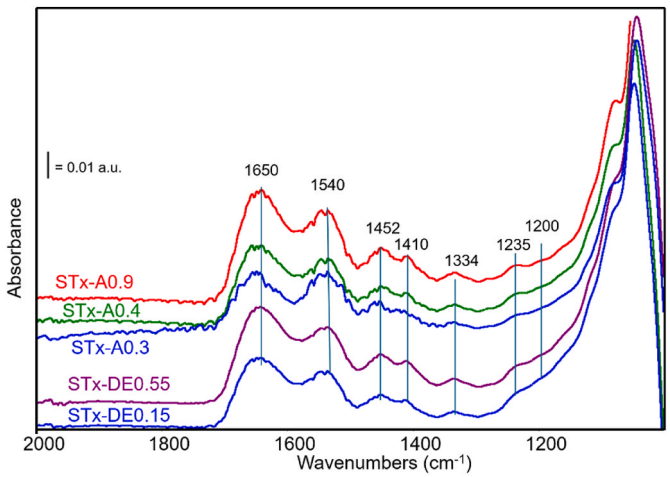

Fig. 5. FTIR-ATR spectra of the organoclays upon the pristine STx spectrum subtraction.

No spectroscopic differences are evident comparing the hybrid materials based on the two hydrolysates ***A*** and ***DE***.

In all the analysed spectra, the two broad bands at 1650 and 1540 cm^{-1} are attributable to the vibration of the peptide bond, namely to the amide I band associated to the carbonyl stretching mode, and to the amide II band, associated to N-H bending and C-N stretching modes.

The weaker and broad band at 1235 cm^{-1} can be due to the amide III band (C-N stretching and N-H bending modes), thus confirming the presence of peptides or polypeptides. Other broad bands at 1450 and 1410 cm^{-1}, also detectable, are likely due to C-H deformation modes in the amino acid chain/molecules, although, according to some literature, they could correspond to the vibrations of the pyrrolidinic rings of proline and hydroxyproline (common amino acids in the collagen structure) and/or to the C-H deformation modes and COO^{-} symmetric stretching modes of glycine, a component of the hydrolysates.

The hydrolysation process can explain the widening of the amide I band due to the denaturation of the collagen, thus leading to less defined amide I and amide II bands. This effect is indeed to be expected, due to the complex nature of the mixture. Moreover, the interaction of the peptide's chains with the STx matrix leads to a further broadening of the amide bands that are shifted to higher (amide I) or lower (amide II) frequencies in comparison to the same bands in the spectrum of reference hydrolysates. This effect points out a significant interaction of the peptide bond with the inorganic matrix.

In the low frequency region of the spectrum, a strong and complex absorption is also observed, growing between 1150 and 1080 cm^{-1}. Bands around these positions have been attributed to C-N stretching vibrations as well as peptide skeletal stretching mode. However, in this region the perturbation of Si-O vibrational modes can appear as positive band, too, suggesting a modification of these sites caused by the interaction with the hydrolysates [57–60]. Accordingly, the presence of free amino acids and/or small peptides interacting with the carrier is further confirmed.

To get further information about HYs location onto the carrier, samples were investigated by SEM-EDX analysis. Results are reported in Fig. 6. Considering SEM images (Fig, 6 a,b), no other features than those of the carrier are distinguishable. However, if EDX analysis is performed, using Nitrogen (N) as tracers, a homogeneous distribution of the organic molecules on all the material is evident (Fig. 6c and d). Nitrogen atoms, indeed, are key component of amino acids and peptides or polypeptides in general, and no evidence of N was found in pristine STx (Fig. S5). Accordingly, no preferential adsorption sites can be inferred in this case.

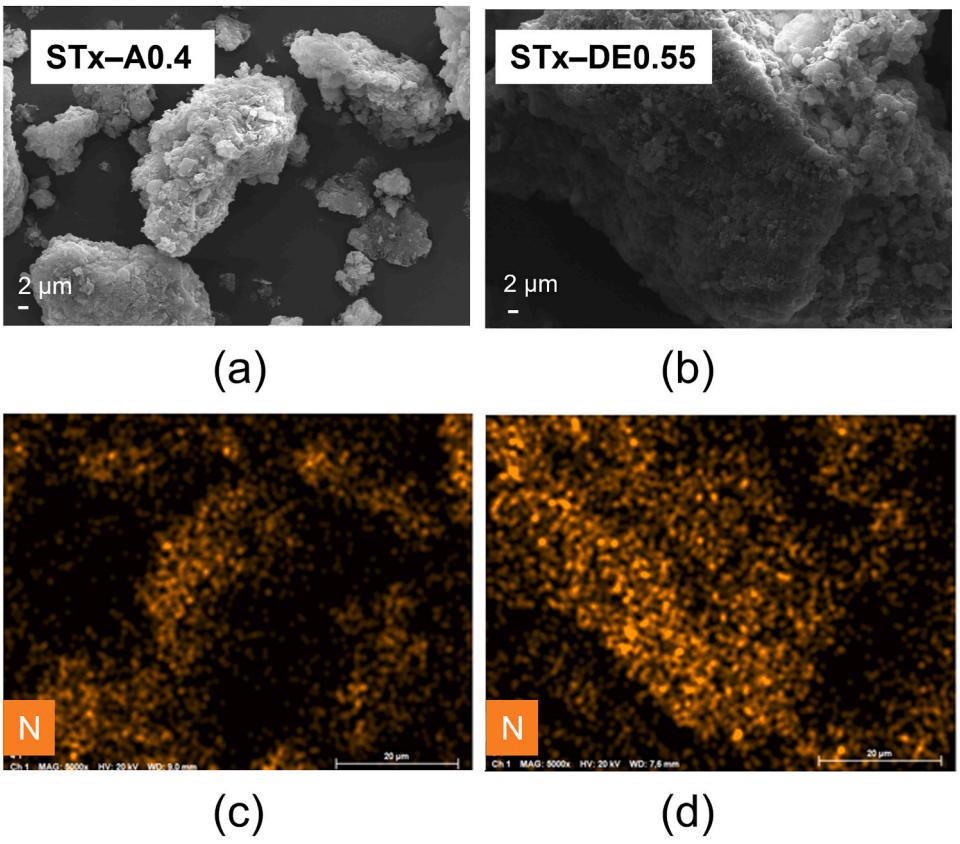

Fig. 6. SEM-EDX analysis (magnification 5000×) of a,c) STx-A0.4, b,d) STx-DE0.55. Dark yellow spots: Nitrogen.

Table 1
Copper capture as a function of initial Cu content for A-based and DE-based organoclays.

A-BASED	Initial Cu content (mmol/g)			DE-BASED	Initial Cu content (mmol/g)		
	0.06	0.38	2		0.06	0.38	2
	Cu uptake (mmol/g)				Cu uptake (mmol/g)		
STx	0.059	0.1	0.54	STx	0.059	0.1	0.54
STx-A0.3	0.057	0.22	0.32	STx-DE0.15	0.058	0.12	0.6
STx-A0.4	0.05	0.21	0.45	STx-DE0.55	0.053	0.21	0.51
STx-A0.9	0.055	0.2	0.45				

3.3. Metal ions capture

3.3.1. Copper uptake

Copper adsorption was performed on pristine STx, and on the synthetized organoclays, namely STx-A0.3, STx-A0.4, STx-A0.9 and on STx-DE0.15 and STx-DE0.55.

Results on copper uptake for the different ***A*** and ***DE*** loadings in the carrier, are plotted in Table 1, respectively.

Both pristine and organoclay systems are able to capture Cu ions, at any tested initial concentration (Table 1). Except for the lowest Cu content (0.06 $mmol_{Cu}/g_{sorbent}$), where a total metal capture was found for all the samples, and in both systems Cu capture almost linearly increased with the initial Cu content in solution. Moreover, the presence of the organoclay generally largely improved the metal capture. This phenomenon is particularly relevant at initial Cu content of 0.38 $mmol_{Cu}/g_{sorbent}$. However, in case of the ***A***-based system, a plateau trend is observed for the sorbents at the higher HY loading (Table 1). On the contrary, no plateau trend was observed in the pristine carrier and in ***DE***-containing materials. In case of ***DE***, only a slight lower adsorption was found when STx-DE0.55 was contacted with the highest initial metal content (Table 1).

The improved metal capture observed in presence of the hydrolysates suggests that metal ions may mainly be captured in the organoclays by their organic part [61]. Therefore, the formation of complexes between the organic part of the organoclay and Cu ions can be hypothesized [21,62]. For instance, the occurrence of metal-hydrolysed interaction in STx-***A*** was immediately evidenced by a change in the sorbent colour already at low Cu initial content, thus irrespective of the captured Cu(II). Indeed, the sorbent colour passes from the light beige of the organoclay (Fig. S10a) to a bright blue tint (Fig. S10b). On the contrary, no special colour changes were found in pristine STx. Such an effect is possibly due to the formation of coordination bonds between the hydrolysate and Cu ions, in particular, via copper glycinate (Cu $(H_2NCH_2COO)_2$ x (H_2O)x) [63] or similar copper-amino-acid complexes formation. The presence of glycine can be inferred considering that the hydrolysate mixture is mainly collagen, where glycine is one the main constituent [30]. Regarding the extent of the phenomenon, little can be said, because it is known that Cu-ammonia complexes are generally highly coloured (due to electrons delocalization) irrespective of Cu content [64].

The presence of the threshold in metal capture, corresponding to a maximum of 0.45 $mmol_{Cu}/g_{sorbent}$, in case of the ***A***-based systems, could

suggest a possible adsorption sites' saturation phenomenon when initial metal concentration is high. This data could be explained considering that the metal and the hydrolysate adsorption sites are the same, which in the organoclays with the higher ***A*** loading are partially occupied by the hydrolysate. As a matter of fact, on increasing the ***A*** loading, both cluttered interlayers and partially occupied surfaces, may hinder Cu adsorption, thus, resulting in a constant metal capture observed at the highest Cu content, and this phenomenon becomes more and more evident on increasing ***A*** loading. Sites competition is not present in case of STx, where all the sites are free for Cu adsorption, and in ***DE***-based, at the tested Cu concentration, suggesting for the presence of lower hindrance effect in this case.

An alternative explanation for the different adsorption behaviours could be found in the pH of the contacting solution. Indeed, pH may affect the capture mechanism due to the competition between a target ion and the protons in solution for the occupation of sorbent sites in the clay mineral [65]. Specifically, the weakly acid sorbent sites are deprotonated when the pH increase, thus favouring Cu capture [66,67].

In our study, the used pH (3.3–4.7) favours the occurrence of Cu^{2+} and $Cu(OH)^{+}$ [68], and positively charged amino acids of the hydrolysate (i.e. pH < IP) in solution. At the same time, the pristine STx is negatively charged [45].

Yuting Chu et al. [65], studying Cu uptake by tyrosine-modified Na-Montmorillonite observed an increase in Cu uptake on increasing pH, reaching a maximum at pH = 5 close to that of our experimental conditions.

A pH range 3.3–3.5 induces the protonation of the amino acids. Intercalated hydrolysates may hamper cation exchange mechanisms, thus contributing to explain the lower extent of the Cu capture with respect to the STx pristine. The higher Cu adsorption by STx (Table 1) may be favoured by the pH value (4.4–4.8) of the solution as also reported in the literature.

In Fig. 7, the XRPD patterns of the adsorbent (pristine STx and ***A***-, ***DE***-organoclays) before and after Cu uptake are compared. The pattern of the STx-Cu0.54 sample shows a broad reflection which is shifted toward higher 2θ angles with respect to the pristine pattern. This suggests a shrinkage of the interlayer site when the montmorillonite is contacted with the Cu solution. The observed interlayer contraction is due to the Ca-Cu exchange mechanism coherently with the Ca concentrations found into the reaction solution (0.22 $mmol_{Ca}/g_{STx}$). There are no significant changes in the Bragg peak positions of the organoclay before and after the Cu uptake (compare the STx-A0.4 with STx-A0.4-Cu0.45 and STX-DE0.55 with STx-DE0.55-Cu0.51). This finding points to no variation in the interlayer site population occurs when the organoclays are contacted with the Cu solutions and only surface adsorption mechanisms are active.

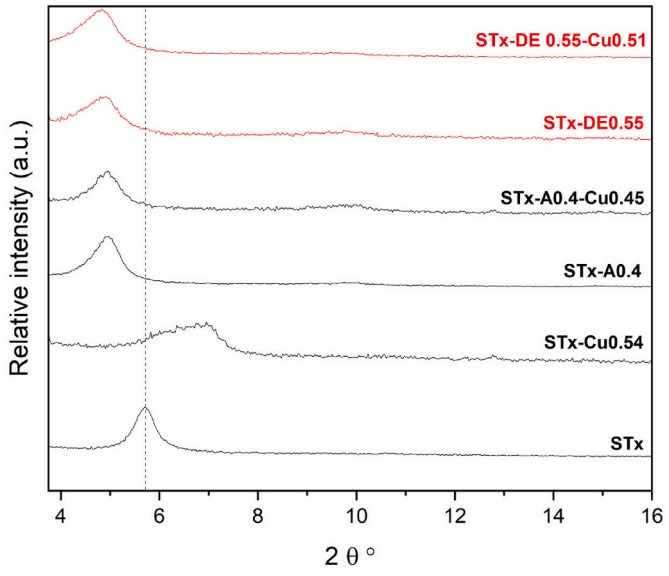

Fig. 7. XRPD patterns of the pristine STx and of the synthetized organoclays before and after Cu capture.

FT-IR data about ***DE***-based hybrids have been recorded after Cu adsorption. Two spectra as examples of each adsorption process are reported in Supporting info (Fig. S12). Very similar features are reported in the spectra of samples STx-***A*** and STx-***DE*** after Cu ions adsorption. Namely, the main bands of the peptide linkage are still evident and slightly broader than in the spectrum of the pristine hybrid system before adsorption. Apparently, a new component is evident at lower frequencies (around 1610 cm^{-1}). Moreover, the amide II band decreases in relative intensity. These observations can be explained by the stronger interaction of N-containing groups with the metal ions but also by the treatment in acidic pH.

Bands of OH groups are also detected as negative features, followed by a broad positive absorption, suggesting that also exposed surface/edges of STx participate to the adsorption process.

Samples were also characterized by SEM-EDX analysis to investigate the possible Cu(II) distribution in organoclays due to the presence of residual amino acids. STx-A0.4 and STx-DE0.55 were analysed and compared with pristine STx (Fig. 8a–h). Nitrogen distribution was considered, being nitrogen one of the main elements, different than carbon, present in the hydrolysates, thus considered as probe; nitrogen was not present in pristine STx.

No difference in the morphology of the samples was appreciable; they are all characterized by a quite similar complex structure (Fig. 8a–c), and they are not distinguishable, in principle by a simple microscopic inspection. Also, EDX, despite being more informative was unable to definitively demonstrate the preferential interaction of Cu with the amino acids. Indeed, in the case of STx-Cu, a homogeneous copper distribution was evident (Blue spots in Fig. 8 d), but also an homogenous copper distribution was observed in the organoclays (Fig. 8e and f); however, in this case, Cu distribution apparently closely resembles the nitrogen distribution (the yellow spots in Fig. 8g–h). Also in this case, such evidence may suggest for a preferential interaction Cu-amino acids, but it was not conclusive.

For this reason, both pristine and organoclays before and after being contacted with the higher copper solution concentration (e.g., 2 $mmol_{Cu}/g_{sorbent}$) were analysed by EPR (Fig. 9a and b).

EPR spectra performed on the samples before Cu^{2+} contact did not show any signals due to Cu(II). In fact, no great differences emerged among pristine STx, STx-A0.4 and STx-DE0.55 (Fig. S11); all the samples showed small signals due the presence of paramagnetic metal traces such as Fe(III) centers at g = 4.3 and Mn(II) evidence by the sextet at g = 2 due to the ^{55}Mn(I = 5/2) hyperfine coupling. Instead, only in STx-DE0.55 a very small signal at about g = 2.02 was detected, not present in the pristine STx neither in the STx-A0.4, which may be ascribed to trace of carbon centred radicals.

Copper adsorption by STx was confirmed by the presence of the typical EPR signal of Cu(II) at $g_{||} = 2{,}34$, $g_{\perp} = 2.09$, and resolved parallel hyperfine structures $A_{||}$ = 176 G upon metal capture and absent in pristine STx (Fig. 9) [69], which can be assigned to Cu(II) centers with tetragonally distorted octahedral symmetry [70]. The preferential interaction of copper with the hydrolysates are suggested by the EPR spectra of STx-A0.3-Cu0.32, 0 STx-A0.4-Cu0.45, STx-DE0.15-Cu0.6, STx-DE055-Cu0.51, obtained after Cu capture. All spectra showed a main Cu(II) signal at $g_{||} = 2.32$, $g_{\perp} = 2.09$, and $A_{||} = 168$, overlapped to other less detectable and slightly different Cu(II) signals with similar features. Also in this case, they can be attributed to Cu(II) centers with tetragonally distorted octahedral symmetry. Moreover, the modifications of g and A values, compared to STx, evidenced a different coordination of the metal, probably due to its interaction with the functional groups of the hydrolysates on the clay surface, thus confirming the hypothesis of Cu-hydrolysate preferential interaction.

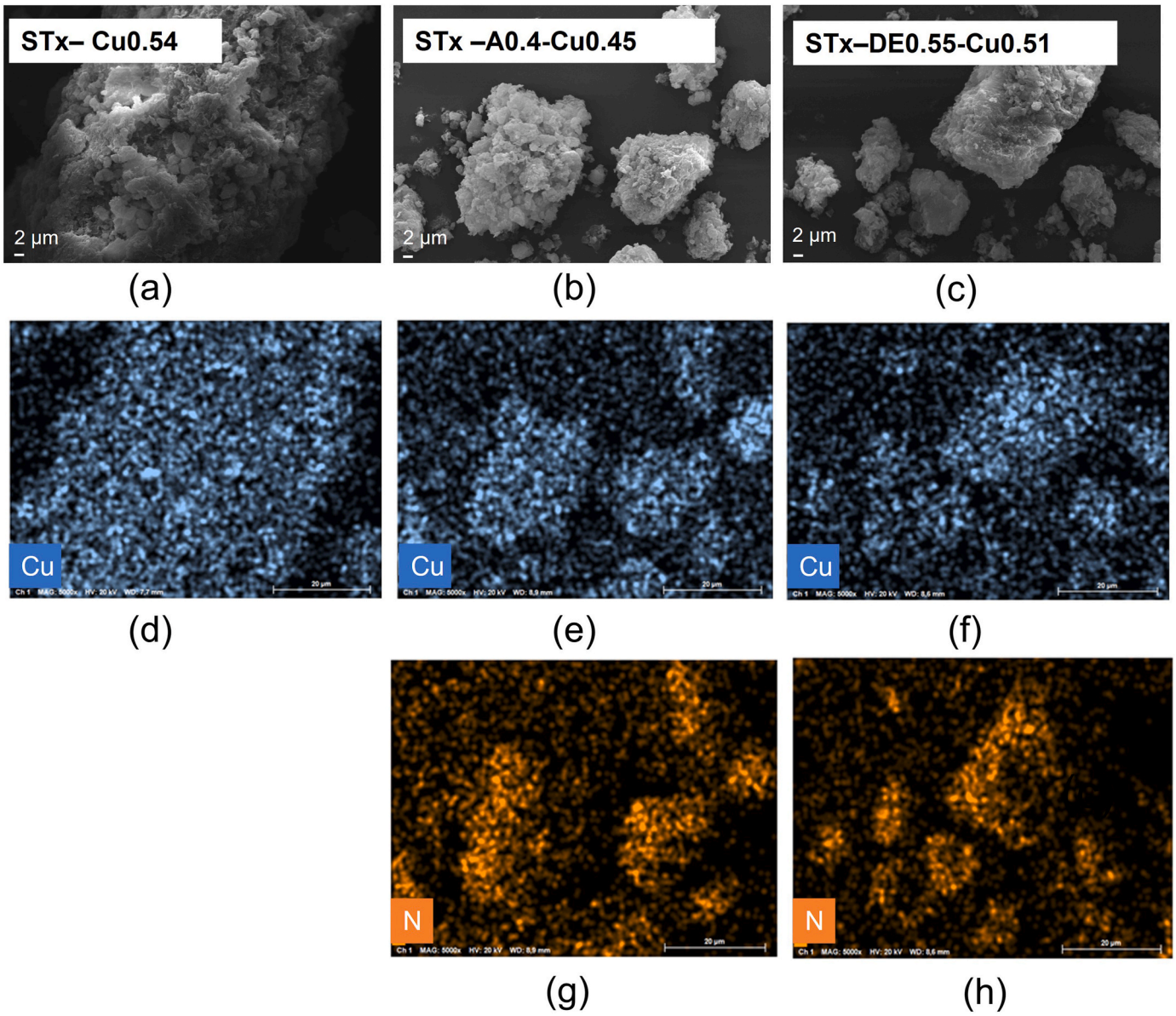

Fig. 8. SEM-EDX analysis (magnification 5000×) of a) STx-Cu0.54, b) STx-A0.4-Cu0.45, c) STx-DE0.55-Cu0.51, d-f) EDX analysis of copper, g-h) EDX analysis of nitrogen.

3.3.2. *Zinc uptake*

Zinc uptake was performed using a concentration of 52 mM (1.04 $mmol_{Zn}/g_{STx}$), i.e., at the Zn concentration in weaning pig manure [10]. Zn solution was contacted with pristine STx, as well as STx-A and STx-DE samples, and results are reported in Table 2. During the experiments, the pH of the Zn suspensions varied between 3.5 and 4.9, as shown in Fig. S13.

Given data of Tables 2 and it is evident that STx-DE samples were always better performing than STx-A. A slight improvement in Zn (II) capture over pristine STx is only observed for the sample STx-DE-0.15. Zn capture is only slightly higher than in pristine STx: 46 % and 45 %, respectively, and a higher HY loading entailed a worsening of the capture performances. Accordingly, functionalization did not make improvement and is potentially detrimental for zinc capture. However, the higher affinity of copper ions for the sorbents here proposed, could have a positive effect when Zn and Cu are co-present, as in real manure, thus pointing out for a possible selective metal capture. However, this point need for further confirmation using mixed solutions first, and real manure, second. In the case of Zn, no broadening of the *d001* reflection was manifests when Zn is contacted with pristine STx (Fig. S14), and calcium release up to 0.15 $mmol_{Ca}/g_{STx}$ was detected during the experiments, suggesting a possible ion exchange mechanism.

FT-IR spectra of A-based and DE-based hybrids have been recorded after Zn adsorption (Fig. S15). Comparable results to copper samples were obtained.

Also in this case, samples were characterized by SEM-EDX analysis (Fig. 10a–h) to investigate Zn (II) distribution in the pristine STx and in the organoclays, STx-A0.4 and STx-DE0.55 (Fig. 10a–c). The samples showed the characteristic complex structure of STx, and no other feature related to Zinc phase were detected. Considering EDX analysis, a homogenous distribution of Zn (II) is evident in all the studied samples (Fig. 10d–f). In this case there is no evident correlation between nitrogen (Fig. 10g–h), and zinc distribution, as in the case of copper. Indeed, in the presence of the organoclay, zinc seems to be equally distributed between the inorganic component (i.e., STx) and the organic one (i.e. the hydrolysed).

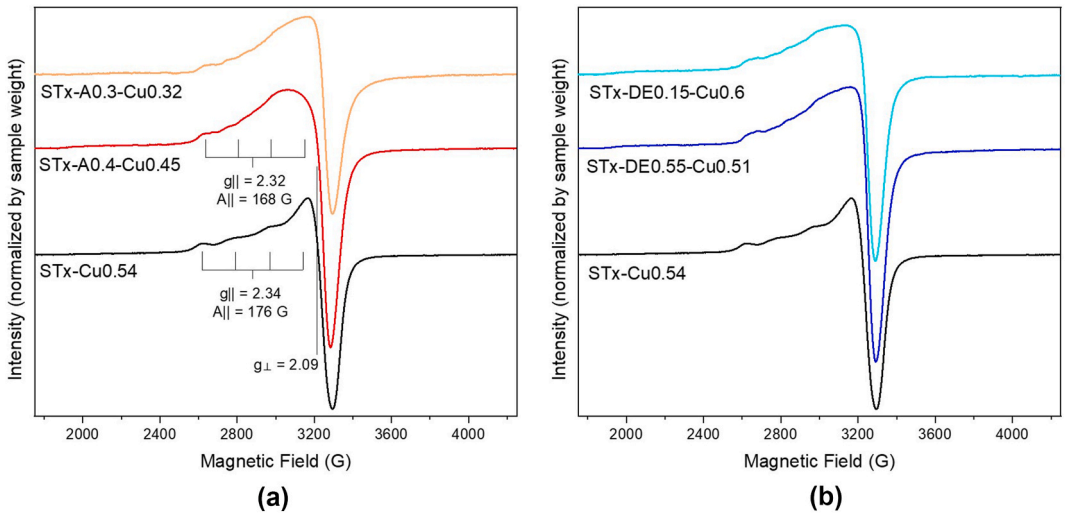

Fig. 9. EPR spectra of a) STx–Cu0.54, STx-A0.4-Cu0.45, STx-A0.3-Cu0.32, b) STx-Cu 0.54, STx–DE0.55-Cu0.51, STx–DE0.15-Cu0.6, normalized by sample weight.

Table 2
Zn Capture by the different sorbents.

A-BASED	Initial Zn content (mmol/g)	DE-BASED	Initial Zn content (mmol/g)
	1.04		1.04
	Zn uptake (mmol/g)		Zn uptake (mmol/g)
STx	0.45	STx	0.45
STx-A0.3	0.34	STx-DE0.15	0.47
STx-A0.4	0.29	STx-DE0.55	0.32

4. Conclusions and final considerations

In this study two hydrolysed leather flashings, a mixture of amino acids in single amino acids or in peptides, namely A and DE hydrolysates were used to modify Ca-Montmorillonite clay (STx). The experiments verified that STx can load the two hydrolysed amino acid solutions (A and DE) within 90 min contact time and without pH modifications. A nonlinear adsorption phenomenon was verified for A hydrolysate, with an adsorption plateau at 0.44 $mmol_{HY}/g_{STx}$, for an initial contacting content set at 1.8 $mmol_{HY}/g_{STx}$. Increasing A initial content an almost linear adsorption is present. Instead, DE adsorption follows a linear adsorption behaviour. According to XRPD analysis, a shift of the d001 reflection towards lower angles is manifested, compatible with an maxium interlayer expansion of 3.03 Å in the STx-A0.4 sample, corresponding to an A loading of 0.44 $mmol_A/g_{STx}$. No further expansion was observed by increasing the HY content. This testifies for concomitant intercalation of amino acids and surface adsorption phenomena. The same trend in the peak positions was observed for STx-DE samples although a lower interlayer increment was measured with respect to A-organoclay.

The TG-DTG analysis further confirms the presence of organic ligands in the organoclays, as it indicates decompositions, that are not present in pristine STx, occurring at high temperatures in the range of 350–500 °C, in line with the decomposition of collagen which is a main component of HY. FT-IR data suggest in both cases a strong interaction between the clay matrix and the HYs through the amide group. Nevertheless, features due to the peptidic chain are still well evident thus the molecular structure of the organic molecule is not affected.

The resultant organoclays HY-STx were tested for the capture of Cu and Zn, which are present in pig manure. Three different Cu stock concentrations were used, corresponding to 0.06, 0.38 and 2.00 $mmol_{Cu}/g_{STx}$. For the lowest copper content (0.06 $mmol_{Cu}/g_{STx\text{-}A}$) a near total Cu capture (capture efficiency in the range of 83–98 %) is observed for all tested sorbent solids, independent on HYs nature or loading concentration. At 0.38 $mmol_{Cu}/g_{STx}$, a larger Cu capture occurs upon increase of A and DE loadings (capture efficiency in the range of 32-58 %) compared to the pristine clay (capture efficiency of 26 %). Concerning 2.00 $mmol_{Cu}/g_{STx}$, a site saturation is reached for both A and DE hydrolysates, corresponding to a maximum Cu capture of 0.45 $mmol_{Cu}/g_{STxA}$ and 0.6 $mmol_{Cu}/g_{STxDE}$, equal to a capture efficiency of 22 % and 30 % respectively. In case of Zn, only one concentration was tested, corresponding to the initial absolute content set at 1.04 $mmol_{Zn}/g_{STx}$. However, HY loading was detrimental to the adsorption of Zn compared to pristine clay (capture efficiency of 28 %), indicating site hindrance.

It is undeniable that the preliminary results here reported demonstrated how protein hydrolysates derived from leather tanning wastes are effective clay modifiers to obtain sorbents to treat streams contaminated by Cu, but not Zn. Therefore, the interaction between the hydrolysate and the clay, and between the organoclay and the metal ions, are necessary to better explain the interaction and the capture mechanism to tune the capture capacity of the system. Moreover, the capture capability towards other typical water pollutants, such as for instance Pb, Cr or Cd, has to be assessed to more generalize utilisation of these new materials. Similarly, the possibility of reuse the spent sorbents or to dispose them in a safer manner has to be considered and study to possibly “close the circle”.

However, the authors believe that the value of this study does not lie in the development of an adsorbent with outstanding properties, capable of replacing the existing commercial alternatives, but rather in the adoption of a circular approach to the problem. The reduction of hazardous waste through its re-use, together with the possibility of producing a material without the use of natural resources and with minimal carbon dioxide emissions, represents a highly promising strategy in terms of both cost-efficiency and low environmental impact.

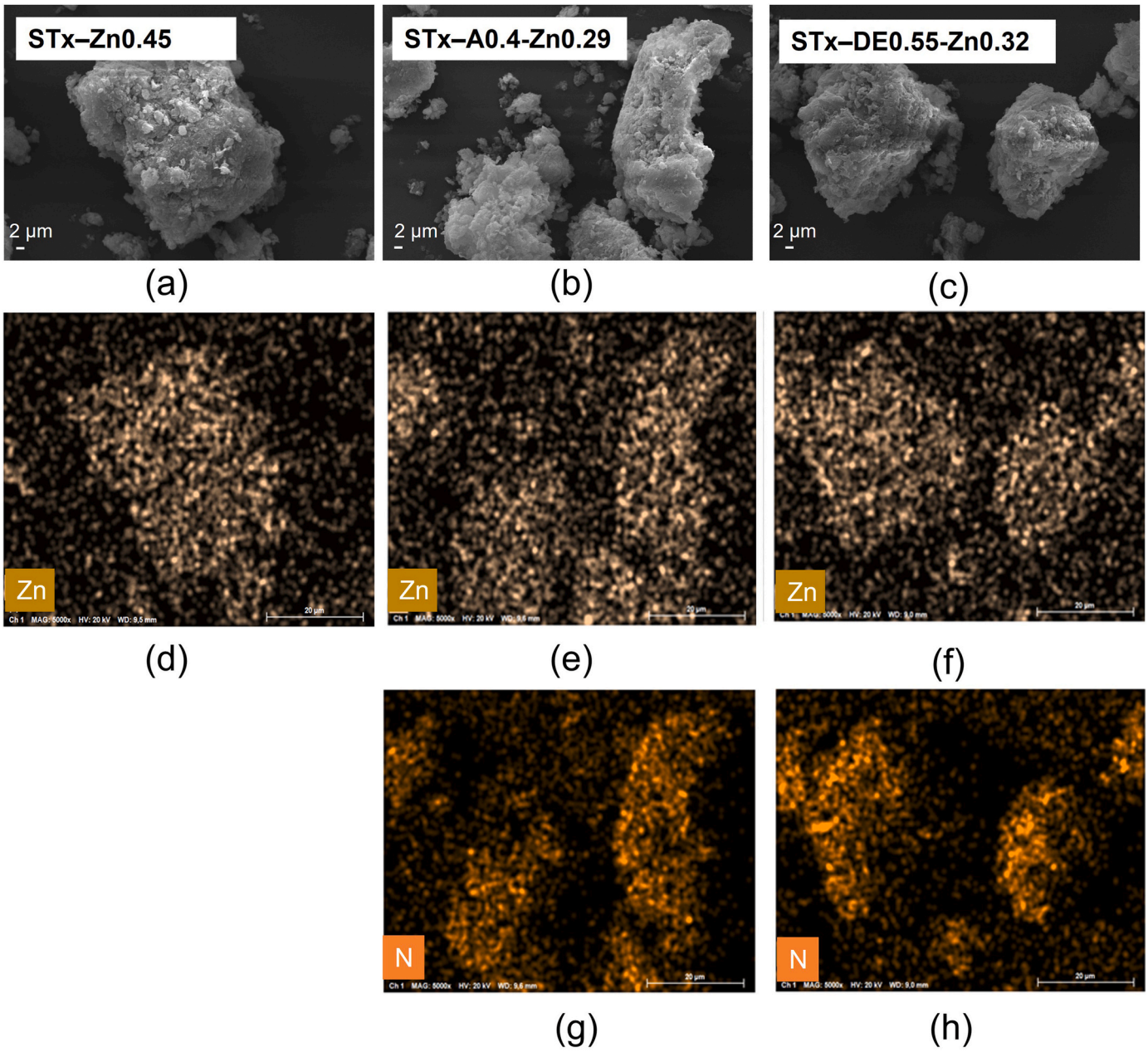

Fig. 10. SEM-EDX analysis (magnification of 5000×) of a) STx- Zn0.45, b) STx-A0.4-Zn0.29, c) STx-DE0.55-Zn0.32, d-f) EDX analysis of zinc, g-h) EDX analysis of nitrogen.

CRediT authorship contribution statement

Marianna Guagliano: Writing – review & editing, Writing – original draft, Visualization, Methodology, Investigation, Formal analysis, Data curation, Conceptualization. **Andrea Tong Hua Borgonovo:** Writing – review & editing, Visualization, Investigation, Formal analysis, Data curation. **Silvia Mostoni:** Writing – review & editing, Visualization, Resources, Methodology, Investigation, Formal analysis. **Maria Lacalamita:** Writing – review & editing, Visualization, Resources, Methodology, Investigation. **Ernesto Mesto:** Writing – review & editing, Visualization, Resources, Methodology, Investigation. **Elisabetta Finocchio:** Writing – review & editing, Visualization, Resources, Methodology, Investigation. **Giovanni Dotelli:** Writing – review & editing, Resources, Formal analysis, Supervision, Validation. **Emanuela Schingaro:** Writing – review & editing, Resources, Methodology. **Stefania Lupinelli:** Writing – review & editing, Resources, Data curation, Methodology, Visualization. **Serena Reggi:** Writing – review & editing, Visualization, Resources, Investigation, Validation. **Matteo Dell'Anno:** Writing – review & editing, Visualization, Resources, Investigation, Validation. **Luciana Rossi:** Writing – review & editing, Visualization, Resources, Investigation, Validation. **Roberto Scotti:** Writing – review & editing, Visualization, Resources, Formal analysis, Investigation. **Maurizio Bellotto:** Writing – review & editing, Visualization, Supervision, Methodology, Investigation, Conceptualization. **Cinzia Cristiani:** Writing – review & editing, Writing – original draft, Visualization, Validation, Supervision, Resources, Formal analysis, Data curation, Conceptualization.

Declaration of competing interest

The authors declare that they have no known competing financial interests or personal relationships that could have appeared to influence

the work reported in this paper.

Appendix A. Supplementary data

Supplementary data to this article can be found online at https://doi.org/10.1016/j.rsurfi.2025.100645.

Data availability

Data will be made available on request.

References

[1] COMMISSION IMPLEMENTING REGULATION (EU) 2016/1095 - of 6 July 2016 - concerning the Authorisation of Zinc Acetate Dihydrate, Zinc Chloride Anhydrous, Zinc Oxide, Zinc Sulphate Heptahydrate, Zinc Sulphate Monohydrate, Zinc Chelate of Amino Acids Hydrate, Zinc Chelate of Protein Hydrolysates, Zinc Chelate of Glycine Hydrate (Solid) and Zinc Chelate of Glycine Hydrate (Liquid) as Feed Additives for all Animal Species and Amending Regulations (EC) No 1334/2003, (EC) No 479/2006, (EU) No 335/2010 and Implementing Regulations (EU) No 991/2012 and (EU) No 636/2013, (n.d.).

[2] Commission Implementing Regulation (EU) 2023/… of 29 June 2023 Concerning the Renewal of the Authorisation of Copper Chelate of Hydroxy Analogue of Methionine as a Feed Additive for all Animal Species and Repealing Regulation (EU) No 349/2010, (n.d.).

[3] Regulation (EU) 2019/of the European Parliament and of the Council of 11 December 2018 on the Manufacture, Placing on the Market and Use of Medicated Feed, Amending Regulation (EC) No 183/2005 of the European Parliament and of the Council and Repealing Council Directive 90/167/EEC, (n.d.).

[4] Regulation (EU) 2019/of the European Parliament and of the Council of 11 December 2018 on Veterinary Medicinal Products and Repealing Directive 2001/82/EC, (n.d.).

[5] Commission Delegated Regulation (EU) 2023/905 of 27 February 2023 Supplementing Regulation (EU) 2019/6 of the European Parliament and of the Council as Regards the Application of the Prohibition of Use of Certain Antimicrobial Medicinal Products in Animals or Products of Animal Origin Exported from Third Countries into the Union (Text with EEA Relevance.

[6] Questions and Answers on Veterinary Medicinal Products Containing Zinc Oxide to Be Administered Orally to food-producing Species Outcome of a Referral Procedure Under Article 35 of Directive 2001/82/EC (EMEA/V/A/118).

[7] López-Gálvez, G., López-Alonso, M., Pechova, A., Mayo, B., Dierick, N., Gropp, J., 2021. Alternatives to antibiotics and trace elements (copper and zinc) to improve gut health and zootechnical parameters in piglets: a review. Anim. Feed Sci. Technol. 271, 114727. https://doi.org/10.1016/j.anifeedsci.2020.114727.

[8] Jiang, B., Tian, J., Chen, H., Zheng, H., Xu, Z., Lin, Y., 2022. Heavy metals migration and antibiotics removal in anaerobic digestion of swine manure with biochar addition. Environ. Technol. Innovat. 27, 102735. https://doi.org/10.1016/j.eti.2022.102735.

[9] Liu, C., Zhuang, J., Xue, J., Peng, M., Zhang, W., Mao, L., 2023. Passivation mechanism of Cu and Zn with the introduction of composite passivators during anaerobic digestion of pig manure. Bioresour. Technol. 369, 128360. https://doi.org/10.1016/j.biortech.2022.128360.

[10] Hejna, M., Moscatelli, A., Onelli, E., Baldi, A., Pilu, S., Rossi, L., 2019. Evaluation of concentration of heavy metals in animal rearing system. Ital. J. Anim. Sci. 18, 1372–1384. https://doi.org/10.1080/1828051X.2019.1642806.

[11] Duan, B., Feng, Q., 2021. Comparison of the potential ecological and human health risks of heavy metals from sewage sludge and livestock manure for agricultural use. Toxics 9, 145. https://doi.org/10.3390/toxics9070145.

[12] Rai, P.K., Lee, S.S., Zhang, M., Tsang, Y.F., Kim, K.-H., 2019. Heavy metals in food crops: health risks, fate, mechanisms, and management. Environ. Int. 125, 365–385. https://doi.org/10.1016/j.envint.2019.01.067.

[13] Briffa, J., Sinagra, E., Blundell, R., 2020. Heavy metal pollution in the environment and their toxicological effects on humans. Heliyon 6, e04691. https://doi.org/10.1016/j.heliyon.2020.e04691.

[14] Zhen, H., Jia, L., Huang, C., Qiao, Y., Li, J., Li, H., Chen, Q., Wan, Y., 2020. Long-term effects of intensive application of manure on heavy metal pollution risk in protected-field vegetable production. Environ. Pollut. 263, 114552. https://doi.org/10.1016/j.envpol.2020.114552.

[15] Raman, G.S.S., Klima, M.S., 2018. The use of zeolite-based additives for immobilising iron during pressure filtration of coal refuse slurry. J. Environ. Sci. Health Part A 54 (1), 30–38. https://doi.org/10.1080/10934529.2018.1507219.

[16] Celis, R., Hermosín, M.C., Cornejo, J., 2000. Heavy metal adsorption by functionalized clays. Environ. Sci. Technol. 34, 4593–4599. https://doi.org/10.1021/es000013c.

[17] Saffaj, N., Loukili, H., Younssi, S.A., Albizane, A., Bouhria, M., Persin, M., Larbot, A., 2004. Filtration of solution containing heavy metals and dyes by means of ultrafiltration membranes deposited on support made of Moroccan clay. Desalination 168, 301–306. https://doi.org/10.1016/j.desal.2004.07.013.

[18] De Paiva, L.B., Morales, A.R., Valenzuela Díaz, F.R., 2008. Organoclays: properties, preparation and applications. Appl. Clay Sci. 42, 8–24. https://doi.org/10.1016/j.clay.2008.02.006.

[19] Guégan, R., 2018. Organoclay applications and limits in the environment. C. R. Chim. 22, 132–141. https://doi.org/10.1016/j.crci.2018.09.004.

[20] Guo, Y.X., Liu, J.H., Gates, W.P., Zhou, C.H., 2020. Organo-modification of montmorillonite. Clays Clay Miner. 68, 601–622. https://doi.org/10.1007/s42860-020-00098-2.

[21] Boahen, C., Wiafe, S., Owusu, F., Bian, L., 2023. Adsorption of heavy metals from mine wastewater using amino-acid modified Montmorillonite. Sustain. Environ. 9, 2152590. https://doi.org/10.1080/27658511.2022.2152590.

[22] Dashman, T., Stotzky, G., 1982. Adsorption and binding of amino acids on homoionic montmorillonite and kaolinite. Soil Biol. Biochem. 14 (5), 447–456. https://doi.org/10.1016/0038-0717(82)90103-1, 1982.

[23] Pires, J., Jużków, J., Pinto, M.L., 2018. Amino acid modified montmorillonite clays as sustainable materials for carbon dioxide adsorption and separation. Colloids Surf. A Physicochem. Eng. Asp. 544, 105–110. https://doi.org/10.1016/j.colsurfa.2018.02.019.

[24] Ramos, M.E., Huertas, F.J., 2013. Adsorption of glycine on montmorillonite in aqueous solutions. Appl. Clay Sci. 80–81, 10–17. https://doi.org/10.1016/j.clay.2013.05.007.

[25] Block, K.A., Trusiak, A., Katz, A., Alimova, A., Wei, H., Gottlieb, P., Steiner, J.C., 2015. Exfoliation and intercalation of montmorillonite by small peptides. Appl. Clay Sci. 107, 173–181. https://doi.org/10.1016/j.clay.2015.01.021.

[26] Zhu, T.T., Zhou, C.H., Kabwe, F.B., Wu, Q.Q., Li, C.S., Zhang, J.R., 2019. Exfoliation of montmorillonite and related properties of clay/polymer nanocomposites. Appl. Clay Sci. 169, 48–66. https://doi.org/10.1016/j.clay.2018.12.006.

[27] Ding, W., Liu, H., Hao, X., Dong, L., Pang, X., Ding, Z., 2022. Conversion of waste non-chrome metal complex tanned leather shavings to dual-functional bio-additive for the high-performance biomass-derived aldehyde tanned leather processing. Mater. Today Sustain. 17, 100107. https://doi.org/10.1016/j.mtsust.2021.100107.

[28] Cabeza, L.F., Taylor, M.M., DiMaio, G.L., Brown, E.M., Marmer, W.N., Carrió, R., Celma, P.J., Cot, J., 1998. Processing of leather waste: pilot scale studies on chrome shavings. Isolation of potentially valuable protein products and chromium. Waste Manag. 18, 211–218. https://doi.org/10.1016/S0956-053X(98)00032-4.

[29] John Sundar, V., Gnanamani, A., Muralidharan, C., Chandrababu, N.K., Mandal, A. B., 2011. Recovery and utilization of proteinous wastes of leather making: a review. Rev. Environ. Sci. Biotechnol. 10, 151–163. https://doi.org/10.1007/s11157-010-9223-6.

[30] Ammasi, R., Victor, J.S., Chellan, R., Chellappa, M., 2020. Amino acid enriched proteinous wastes: recovery and reuse in leather making. Waste Biomass Valor 11, 5793–5807. https://doi.org/10.1007/s12649-019-00912-6.

[31] Puhazhselvan, P., Pandi, A., Sujiritha, P.B., Antony, G.S., Jaisankar, S.N., Ayyadurai, N., Saravanan, P., Kamini, N.R., 2022. Recycling of tannery fleshing waste by a two step process for preparation of retanning agent. Process Saf. Environ. Prot. 157, 59–67. https://doi.org/10.1016/j.psep.2021.11.003.

[32] Sariatli, F., 2017. Linear economy versus circular economy: a comparative and analyzer Study for optimization of economy for sustainability. Visegrad J. Bioecon. Sustain. Dev. 6, 31–34. https://doi.org/10.1515/vjbsd-2017-0005.

[33] Zampori, L., Stampino, P.G., Cristiani, C., Cazzola, P., Dotelli, G., 2010. Intercalation of poly(ethylene-oxides) in montmorillonite: Tailor-Made nanocontainers for drug delivery systems. Appl. Clay Sci. 50, 266–270. https://doi.org/10.1016/j.clay.2010.08.009.

[34] Martin, E., Robert, T., 1980. Data handbook for clay materials and other non-metallic minerals, edited by H. van Olphen and J. J. Fripiat, pergamon press, Oxford and Elmsford, New York, 1979, 346 + Xiv Pp. Clays Clay Miner. 28 (2), 160. https://doi.org/10.1346/CCMN.1980.0280215, 160.

[35] Jeans, C.V., 1998. MOORE, D. M. & REYNOLDS, R. C., jr. 1997. X-Ray Diffraction and the Identification and analysis of clay minerals, 2nd Ed. Xviii + 378 Pp. Oxford, New York: Oxford University Press. (Spiral-Bound Paperback). ISBN 0 19 508713 5. Geol. Mag. 135 (6), 819–842. https://doi.org/10.1017/S0016756898501501.

[36] Zampori, L., Stampino, P.G., Cristiani, C., Dotelli, G., Cazzola, P., 2010. Synthesis of organoclays using non-ionic surfactants: effect of time, temperature and concentration. Appl. Clay Sci. 48, 97–102. https://doi.org/10.1016/j.clay.2009.11.015.

[37] O'Dell, J.W., 1996. The determination of Chemical Oxygen Demand by semi-automated colorimetry. In: Methods for the Determination of Metals in Environmental Samples. Elsevier, pp. 509–521. https://doi.org/10.1016/B978-0-8155-1398-8.50029-X.

[38] Iannicelli-Zubiani, E.M., Cristiani, C., Dotelli, G., Gallo Stampino, P., Pelosato, R., Mesto, E., Schingaro, E., Lacalamita, M., 2015. Use of natural clays as sorbent materials for rare Earth ions: materials characterization and set up of the operative parameters. Waste Manag. 46, 546–556. https://doi.org/10.1016/j.wasman.2015.09.017.

[39] Zampori, L., Dotelli, G., Gallo Stampino, P., Cristiani, C., Zorzi, F., Finocchio, E., 2012. Thermal characterization of a montmorillonite, modified with polyethylene-glycols (PEG1500 and PEG4000), by in situ HT-XRD and FT IR: formation of a high-temperature phase. Appl. Clay Sci. 59–60, 140–147. https://doi.org/10.1016/j.clay.2012.02.015.

[40] Derkowski, A., Kuligiewicz, A., 2022. Thermal analysis and thermal reactions of smectites: a review of methodology, mechanisms, and kinetics. Clays Clay Miner. 70, 946–972. https://doi.org/10.1007/s42860-023-00222-y.

[41] Nazdracheva, T., Morozov, A., Yavna, V., Kochur, A., 2022. Study of hydration of kaolinite and montmorillonite mixture by IR spectroscopy. J. Mol. Struct. 1250, 131871. https://doi.org/10.1016/j.molstruc.2021.131871.

[42] Kalra, S., Pant, C.K., Pathak, H.D., Mehata, M.S., 2003. Studies on the adsorption of peptides of glycine/alanine on montmorillonite clay with or without co-ordinated divalent cations. Colloids Surf. A Physicochem. Eng. Asp. 212, 43–50. https://doi.org/10.1016/S0927-7757(02)00288-1.

[43] Assifaoui, A., Huault, L., Maissiat, C., Roullier-Gall, C., Jeandet, P., Hirschinger, J., Raya, J., Jaber, M., Lambert, J.-F., Cayot, P., Gougeon, R.D., Loupiac, C., 2014. Structural studies of adsorbed protein (betalactoglobulin) on natural clay (montmorillonite). RSC Adv. 4, 61096–61103. https://doi.org/10.1039/C4RA11607K.

[44] Parbhakar, A., Cuadros, J., Sephton, M.A., Dubbin, W., Coles, B.J., Weiss, D., 2007. Adsorption of l-lysine on montmorillonite. Colloids Surf. A Physicochem. Eng. Asp. 307, 142–149. https://doi.org/10.1016/j.colsurfa.2007.05.022.

[45] Au, P.-I., Leong, Y.-K., 2016. Surface chemistry and rheology of slurries of kaolinite and montmorillonite from different sources. KONA 33, 17–32. https://doi.org/10.14356/kona.2016007.

[46] Y.-K. Leong, Microstructure and time-dependent behavior of STx-1b calcium montmorillonite suspensions, Clays Clay Miner. (n.d.).

[47] Lagaly, G., Ogawa, Makoto, Dekany, I., 2013. Clay mineral–organic interactions. In: Handbook of Clay Science Part A: Fundamentals, second ed., 5, pp. 437–505. https://doi.org/10.1016/B978-0-08-098258-8.00015-8.

[48] Chu, Y., Khan, M.A., Wang, F., Xia, M., Lei, W., Zhu, S., 2019. Kinetics and equilibrium isotherms of adsorption of Pb(II) and Cu(II) onto raw and arginine-modified montmorillonite. Adv. Powder Technol. 30, 1067–1078. https://doi.org/10.1016/j.apt.2019.03.002.

[49] Zhang, Z.Z., Sparks, D.L., Scrivner, N.C., 1993. Sorption and desorption of Quaternary amine cations on clays. Environ. Sci. Technol. 27, 1625–1631. https://doi.org/10.1021/es00045a020.

[50] Balek, V., Beneš, M., Šubrt, J., Pérez-Rodriguez, J.L., Sánchez-Jiménez, P.E., Pérez-Maqueda, L.A., Pascual-Cosp, J., 2008. Thermal characterization of montmorillonite clays saturated with various cations. J. Therm. Anal. Calorim. 92, 191–197. https://doi.org/10.1007/s10973-007-8761-9.

[51] Lv, G., Li, Z., Jiang, W.-T., Chang, P.-H., Liao, L., 2015. Interlayer configuration of ionic liquids in a Ca-montmorillonite as evidenced by FTIR, TG-DTG, and XRD analyses. Mater. Chem. Phys. 162, 417–424. https://doi.org/10.1016/j.matchemphys.2015.06.008.

[52] Türk, S., Altınsoy, I., Çelebi Efe, G., Ipek, M., Özacar, M., Bindal, C., 2018. 3D porous collagen/functionalized multiwalled carbon nanotube/chitosan/hydroxyapatite composite scaffolds for bone tissue engineering. Mater. Sci. Eng. C 92, 757–768. https://doi.org/10.1016/j.msec.2018.07.020.

[53] Weiss, I.M., Muth, C., Drumm, R., Kirchner, H.O.K., 2018. Thermal decomposition of the amino acids glycine, cysteine, aspartic acid, asparagine, glutamic acid, glutamine, arginine and histidine. BMC Biophys. 11, 2. https://doi.org/10.1186/s13628-018-0042-4.

[54] Zheng, Y., Wen, X., Wu, J., Wang, L.-N., Yuan, Z., Peng, J., Meng, H., 2015. Immobilization of collagen peptide on dialdehyde bacterial cellulose nanofibers via covalent bonds for tissue engineering and regeneration. IJN 4623. https://doi.org/10.2147/IJN.S84452.

[55] Hoshi, M., Sawada, T., Hatakeyama, W., Taira, M., Hachinohe, Y., Takafuji, K., Kihara, H., Takemoto, S., Kondo, H., 2022. Characterization of five collagenous biomaterials by SEM observations, TG-DTA, collagenase dissolution tests and subcutaneous implantation tests. Materials 15, 1155. https://doi.org/10.3390/ma15031155.

[56] Finocchio, E., Cristiani, C., Dotelli, G., Stampino, P.G., Zampori, L., 2014. Thermal evolution of PEG-Based and BRIJ-Based hybrid organo-inorganic materials. FT-IR studies. Vib. Spectrosc. 71, 47–56. https://doi.org/10.1016/j.vibspec.2013.12.010.

[57] Chang, M.C., Tanaka, J., 2002. FT-IR study for hydroxyapatite/collagen nanocomposite cross-linked by glutaraldehyde. Biomaterials 23, 4811–4818. https://doi.org/10.1016/S0142-9612(02)00232-6.

[58] Guzzi Plepis, A.M.D., Goissis, G., Das-Gupta, D.K., 1996. Dielectric and pyroelectric characterization of anionic and native collagen. Polym. Eng. Sci. 36, 2932–2938. https://doi.org/10.1002/pen.10694.

[59] Kristoffersen, K.A., Liland, K.H., Böcker, U., Wubshet, S.G., Lindberg, D., Horn, S. J., Afseth, N.K., 2019. FTIR-based hierarchical modeling for prediction of average molecular weights of protein hydrolysates. Talanta 205, 120084. https://doi.org/10.1016/j.talanta.2019.06.084.

[60] Marin, M.M., Ianchis, R., Leu Alexa, R., Gifu, I.C., Kaya, M.G.A., Savu, D.I., Popescu, R.C., Alexandrescu, E., Ninciuleanu, C.M., Preda, S., Ignat, M., Constantinescu, R., Iovu, H., 2021. Development of new collagen/clay composite biomaterials. IJMS 23, 401. https://doi.org/10.3390/ijms23010401.

[61] Cristiani, C., Bellotto, M., Dotelli, G., Gallo Stampino, P., Latorrata, S., Finocchio, E., 2022. Capture and Release Mechanism of Ni and La Ions via Solid/Liquid Process: use of Polymer-Modified Clay and Activated Carbons. Polymers 14, 485. https://doi.org/10.3390/polym14030485.

[62] Zhao, F., Yang, S., Xiao, X., Chen, L., Wang, Y., Li, Y., E, T., 2024. Bovine hide collagen/tannin extract composite: a revelation of the selective structure-activity relationship between phenolic hydroxyls and Cu(II) and study on adsorption properties. Colloids Surf. A Physicochem. Eng. Asp. 682, 132886. https://doi.org/10.1016/j.colsurfa.2023.132886.

[63] Azeem, M., Li, K., Qin, Y., Dong, L., Li, W., 2021. Mechanical study of a copper dietary supplement, copper glycinate hydrate. CrystEngComm 23, 1815–1820. https://doi.org/10.1039/D0CE01706J.

[64] Earl, B.L., 1985. The colorful complexes of copper(II). J. Chem. Educ. 62, 798. https://doi.org/10.1021/ed062p798.1.

[65] Chu, Y., Zhu, S., Wang, F., Lei, W., Xia, M., Liao, C., 2019. Tyrosine-immobilized montmorillonite: an efficient adsorbent for removal of Pb^{2+} and Cu^{2+} from aqueous solution. J. Chem. Eng. Data 64, 3535–3546. https://doi.org/10.1021/acs.jced.9b00304.

[66] Bhattacharyya, K.G., Gupta, S.S., 2011. Removal of Cu(II) by natural and acid-activated clays: an insight of adsorption isotherm, kinetic and thermodynamics. Desalination 272, 66–75. https://doi.org/10.1016/j.desal.2011.01.001.

[67] Bhattacharyya, K.G., Gupta, S.S., 2006. Kaolinite, montmorillonite, and their modified derivatives as adsorbents for removal of Cu(II) from aqueous solution. Sep. Purif. Technol. 50, 388–397. https://doi.org/10.1016/j.seppur.2005.12.014.

[68] Cuppett, J.D., 2006. Evaluation of copper speciation and water quality factors that affect aqueous copper tasting response. Chem. Senses 31, 689–697. https://doi.org/10.1093/chemse/bjl010.

[69] Garribba, E., Micera, G., 2006. The determination of the geometry of Cu(II) complexes: an EPR spectroscopy experiment. J. Chem. Educ. 83, 1229. https://doi.org/10.1021/ed083p1229.

[70] Godiksen, A., Stappen, F.N., Vennestrøm, P.N.R., Giordanino, F., Rasmussen, S.B., Lundegaard, L.F., Mossin, S., 2014. Coordination environment of copper sites in Cu-CHA zeolite investigated by electron paramagnetic resonance. J. Phys. Chem. C 118, 23126–23138. https://doi.org/10.1021/jp5065616.